Cancer Letters 420 (2018) 247–258

Contents lists available at ScienceDirect

Cancer Letters

journal homepage: www.elsevier.com/locate/canlet

Original Articles

Reprogramming tumor stroma using an endogenous lipid lipoxin A4 to treat pancreatic cancer

Jonas Schnittert [a, 1], Marcel A. Heinrich [a, 1], Praneeth R. Kuninty [a], Gert Storm [a, b], Jai Prakash [a, c, *]

[a] Section - Targeted Therapeutics, Department of Biomaterials Science and Technology, University of Twente, Enschede, The Netherlands
[b] Department of Pharmaceutics, Utrecht University, Utrecht, The Netherlands
[c] ScarTec Therapeutics BV, Enschede, The Netherlands

ARTICLE INFO

Article history:
Received 10 September 2017
Received in revised form
25 December 2017
Accepted 22 January 2018

Keywords:
Lipoxin A4
Pancreatic stellate cells
Cancer-associated fibroblasts
Pancreatic cancer
Tumor stroma

ABSTRACT

Pancreatic stellate cells (PSCs) are the precursors of cancer-associated fibroblasts (CAFs), which potentiate pancreatic tumor growth and progression. In this study, we investigated whether Lipoxin A4 (LXA4), an endogenous bioactive lipid, can inhibit the differentiation of human PSCs (hPSCs) into CAF-like myofibroblasts and thereby hPSC-induced pro-tumorigenic effects. LXA4 significantly inhibited TGF-β-mediated differentiation of hPSCs by inhibiting pSmad2/3 signalling. Furthermore, treatment with LXA4 abolished the paracrine effects (proliferation and migration of Panc-1 tumor cells) of hPSCs *in vitro*. These data demonstrated that LXA4 can interrupt pro-tumoral paracrine signalling of hPSCs. Furthermore, LXA4 treatment significant decreased the size and growth rate of 3D-heterospheroids comprised of hPSC and Panc-1 and these effects were exhibited due to inhibition of hPSC-induced collagen1 expression. *In vivo*, we examined the therapeutic efficacy of LXA4 in a co-injection (Panc-1 and hPSCs) subcutaneous tumor model. Intriguingly, LXA4 significantly abolished the tumor growth (either injected intratumor or intraperitoneally), attributed to a significant reduction in fibrosis, shown with collagen1 expression. Altogether, this study proposes LXA4 as a potent inhibitor for hPSCs which can be applied to reprogram tumor stroma in order to treat pancreatic cancer.

1. Introduction

Annually, around 90,000 people in Europe and 45,000 people in the U.S. get diagnosed with pancreatic ductal adenocarcinoma (PDAC), the most common form of pancreatic cancer [1]. Patients with PDAC have a 1 year survival rate of 20%, whereas the 5-year survival rate decreases to 7% [1]. In most PDAC, a surgical resection is not feasible, making radiotherapy or cytotoxic chemotherapy the golden standard treatment. However, these treatments are not effective and result in a survival benefit of only a few months [2,3]. One reason of the treatment failure is the abundant desmoplastic reaction in PDAC, also called the tumor stroma, which supports cancer progression, invasion and metastasis [4]. Novel therapeutic approaches for the treatment of PDAC aim to modulate the cellular components of the tumor stroma. Several different studies have shown an anti-tumoral effect by modulating the tumor stroma [5,6], whereas unexpectedly a complete depletion of the stroma genetically was shown to promote tumor growth [7]. Therefore, it has been suggested to dampen the activity of tumor stroma instead of its total depletion to gain therapeutic benefits [8].

Human pancreatic stellate cells (hPSCs) are the main precursors of pancreatic cancer-associated fibroblasts (CAFs), the key drivers of the pancreatic tumor stroma [5,9,10]. Quiescent hPSCs can be found within the connective tissue of the pancreas in low numbers and secrete only small amounts of extracellular matrix (ECM) proteins (e.g. collagen) [11]. In PDAC, quiescent hPSCs become activated, loose their cytoplasmic lipid storing capacity and start secreting

Abbreviations: Human pancreatic stellate cell, hPSC; Cancer-associated fibroblast, CAF; Pancreatic ductal adenocarcinoma, PDAC; Lipoxin A4, LXA4; Lipoxin B4, LXB4; Transforming growth factor β, TGF-β; Platelet-derived growth factor, PDGF; Extra cellular matrix, ECM; α-smooth muscle actin, α-SMA; Collagen1, Col1; Collagen1α1, Col1α1; Conditioned Medium, CM.

* Corresponding author. Section Targeted Therapeutics, Department of Biomaterials Science and Technology, MIRA Institute for Biomedical Technology and Technical Medicine, University of Twente, Zuidhorst 254, 7500 AE Enschede, The Netherlands.
E-mail address: j.prakash@utwente.nl (J. Prakash).

[1] Authors contributed equally to this work.

https://doi.org/10.1016/j.canlet.2018.01.072
0304-3835/

high amounts of ECM components, leading to fibrosis which ultimately presents as a barrier for tumor drug penetration. In addition, differentiated hPSCs secrete various cytokines and growth factors which stimulate tumor cells and other stromal cells in favour of tumor progression [12]. Therefore, inhibition of hPSC activation might be beneficial for the treatment of pancreatic cancer.

Lipoxins are part of a family of inflammation resolving endogenous lipid mediators which are locally secreted by immune cells such as neutrophils and macrophages in response to infection, injury or inflammatory stimuli [13–16]. Lipoxins are synthesized from membrane arachidonic acid via biochemical synthesis by two major routes. The first route of synthesis starts in platelets where leukotriene A4 is converted into lipoxin by 12-LO. The second major route involves the action of either 5-LO in neutrophils and 15-LO in erythrocytes and reticulocytes. Arachidonic acid is converted into 15-hydroperoxyeicosatetraenoic acid (15-HPETE), which is then converted into lipoxin A and lipoxin B [17]. Based on an aspirin-triggered reaction in which aspirin acetylates cyclooxygenase-2 (COX-2) to form 15R-HPETE, and is eventually metabolized by 5-LO epi-lipoxin, lipoxin A4 (LXA4) and lipoxin B4 (LXB4) are formed [18,19]. Lipoxins and epi-lipoxins function by binding to the high-affinity G protein-coupled lipoxin A4 (LXA4) receptor formyl peptide receptor 2 (FPR2)/ALX [14]. Via this route, LXA4 can resolve inflammation already at low nanomolar concentrations and additionally activates anti-bacterial mechanisms [20,21].

There are little evidences that LXA4 may possess anti-fibrotic effects. In mesangial cells in kidney, it inhibited platelet-derived growth factor (PDGF)–dependent TGF-β production, the expression of fibrosis promoting genes in renal mesangial cells [22] and Akt/PKB activation and cell cycle progression in mesangial cells [23]. Additionally, LXA4 attenuated experimental renal fibrosis [24] and inhibited epithelial to mesenchymal transition of renal epithelial cells in proximal tubules [25]. Also, LXA4 has been shown to inhibit connective tissue growth factor-induced proliferation and TGF-β-dependent pro-fibrotic activity in human lung (myo)fibroblast [26,13]. Yet, there is no study showing the inhibitory effects of LXA4 on hPSC differentiation and its impact on pancreatic tumor growth.

Considering the anti-fibrotic activity of LXA4, in this study, we hypothesized that LXA4 might be an interesting biomolecule to inhibit hPSCs activation and their pro-tumorigenic effects. We show that the LXA4 specific receptor FPR2/ALX is overexpressed in activated hPSCs. Furthermore, we demonstrate the inhibitory effect of LXA4 on the hPSC activation, migration and then hPSC-induced paracrine effect on pancreatic cancer cells. Next, we showed the inhibitory effects of LXA4 on the growth and extracellular matrix (ECM) deposition in stromal-rich 3D-heterospheroids. Eventually, we examined the therapeutic efficacy of LXA4 *in vivo* in a co-injection tumor model which resulted in a reduced tumor growth and intra-tumoral ECM deposition after the treatment with LXA4.

2. Materials and methods

2.1. Cells

Primary human pancreatic stellate cells (ScienCell, Carlsbad, USA), were cultured in complete Stellate Cell Medium (supplemented with 2% FBS, 1% Penicillin/Streptomycin and 1% Stellate Cell Growth Supplements (SteCGS)) (ScienCell). Panc-1 cancer cells were cultured in Dulbecco's Modified Eagles medium (DMEM) High Glucose (4.5 g/l) with L-Glutamine (GE Healthcare, Vienna, Austria) supplemented with 10% FBS (Lonza, Verviers, Belgium), 100 μg/ml penicillin/streptomycin (Sigma Aldrich). AsPc-1 cells were cultured in complete RPMI Medium (GE Healthcare, Vienna, Austria) supplemented with 10% FBS (Lonza), 100 μg/ml penicillin/streptomycin (Sigma). The cells were maintained at 37 °C in a humidified 5% CO2 atmosphere.

2.2. Western blot

To evaluate the expression of the LXA4-specific surface receptor FPR2 and the hPSC activation marker α-SMA, hPSCs were seeded into a 12 well plate at a seeding density of 40.000 cells/well. The next day hPSCs were starved for 24 h and subsequently activated with 5 ng/ml TGF-β for 48 h. To evaluate the effect of LXA4 on TGF-β-mediated Smad 2/3 and phosphorylated Smad 2/3 (pSmad2/3) levels in hPSCs, cells were seeded into a 12 well plate at a seeding density of 40.000 cells/well. The cells were starved for 24 h, treated with 10 nM LXA4 (Biomol, Hamburg, Germany) and activated with 5 ng/μl TGF-β for 30 min. In general, cells were lysed using 1× SDS-lysis buffer, cell lysis was centrifuged at 10,000 g for 10 min, and the supernatant was collected for Western blot analysis. To analyse the expression of MMP-2 in conditioned medium, 1 ml conditioned medium was freeze dried using an Il-Shin TFD5503 Freeze Dryer (Scala Scientific, Ede, The Netherlands) and afterwards resuspended in 100 μl TBS (Thermo Scientific, Rockford, USA). Conditioned medium was mixed with Sample Reducing agent (Life Technologies, Carlsbad, USA) and LDS Sample Buffer (Life Technologies) and incubated at 95 °C for 10 min. Protein lysates and conditioned medium was loaded on a 10% Tris-Glycine gel (Thermo Scientific) and transferred onto PVDF membranes (Thermo Scientific). The blots were incubated with the required primary antibody (Supplementary Table 1) and incubated overnight at 4 °C, followed by incubation with species specific horseradish peroxidase (HRP) conjugated secondary and tertiary antibody for 1 h at RT. Proteins were detected with Pierce™ ECL Plus Western Blotting Substrate kit (Thermo Scientific) and exposed to FluorChem™ M System (ProteinSimple, San José, USA). The protein levels were quantified using Image J software (NIH, MD). To evaluate the amount of Smad 2/3 phosphorylation a pSmad 2/3/Smad 2/3 ratio was calculated.

2.3. Immunocytochemistry

To evaluate the effect of LXA4 on the expression of αSMA and collagen1 (Col1), hPSCs were seeded into a 24 well plate at a seeding density of 5.000 cells/well. The cells were starved, treated with 0.1, 1 and 10 nM LXA4 and TGF-β activated for 48 h. Next, cells were fixed and immunostained for αSMA, and collagen1 as described elsewhere [27]. Stained images were quantified for their positively stained area using ImageJ software.

To evaluate the effect of LXA4 on Smad2/3 and pSmad2/3 expression, hPSCs were seeded into a 24 well plate at a seeding density of 10.000 cells/well. The cells were starved and activated with TGF-β as described previously. After 30 min of incubation with TGF-β, cells were washed with phosphate buffered saline (PBS) (Lonza, Verviers, Belgium) and fixed with 4% paraformaldehyde (Sigma Aldrich) at room temperature for 10 min. Next, cells were washed 3 times with PBS and permeabilized with ice cold HPLC grade methanol (Fisher Scientific) at −20 °C for 10 min. After washing 3 times with PBS cells were blocked with blocking buffer consisting of 1 vol % bovine-serum albumin (BSA) (VWR, Radnor, PA, USA) + 0.3 vol % Triton-X (Sigma Aldrich) in PBS for 1 h. Subsequently, the cells were incubated with monoclonal anti-Smad2/3 or monoclonal anti-pSmad2/3 primary antibodies diluted in blocking buffer and incubated over night at 4 °C. Next, cells were washed 3 times with PBS and incubated with fluorescent secondary antibodies diluted in blocking buffer for 1 h at RT. Cells were washed once with PBS and stained for DAPI by incubation with NucBlue Fixed Cell Stain ReadyProbes Reagent (Life Technologies),

diluted in PBS as described in the manufacturer's instructions, for 5 min. The NuCBlue solution was replaced with PBS and the cells imaged for Alexa Fluor 488 (ex. 495/em. 520) and DAPI (ex. 360/em. 460) using an EVOS FI fluorescent microscope (Life Technologies). Staining of pSmad2/3 was quantified by counting the total number and the number of pSmad 2/3 positive nuclei.

2.4. F-actin staining

To analyse the effect of LXA4 on the F-actin organization of TGF-β activated hPSCs, hPSCs were seeded into 24 well plates at a seeding density of 2.500 cells/well. After 24 h of incubation with 10 nM LXA4 and / or 5 ng/ml TGF-β, cells were washed three times with PBS and subsequently fixed in PBS containing 10% formaldehyde (Sigma Aldrich) for 15 min. After permeabilizing the cells with 0.1 M Triton X-100 (Sigma Aldrich) for 5 min, F-actin was stained with phalloidin (Life Technologies) at a concentration of 250 ng/ml for 30 min. Next, cells were washed with PBS and imaged for phalloidin at (ex. 540/em. 565) using an EVOS FI fluorescent microscope (Life Technologies).

2.5. Quantitative real time PCR

To evaluate the effect of LXA4 on TGF-β-mediated hPSCs activation, cells were seeded into a 12 well plate at a seeding density of 40.000 cells/well. The cells were starved for 24 h, treated with 10 nM LXA4 and activated with 5 ng/μl TGF-β. 24 h after activation total RNA was isolated using the GenElute™ Mammalian Total RNA Miniprep Kit (Sigma Aldrich) and the RNA amount was measured by a NanoDrop® ND-1000 Spectrophotometer (Thermo Scientific). Subsequently, cDNA was synthesized with iScript™ cDNA Synthesis Kit (BioRad, Veenendaal, The Netherlands). 10 ng cDNA were used for each PCR reaction. The real-time PCR primers (Table 1) were purchased from (Sigma Aldrich). Quantitative real time PCR was performed with the 2x SensiMix SYBR and Fluorescein Kit (Bioline GmbH, Luckenwalde, Germany) using a BioRad CFX384 Real-Time PCR detection system (BioRad). Gene expression levels were normalized to the expression of the house-keeping gene RPS18.

2.6. Conditioned media

To collect hPSC conditioned medium, cells were seeded into a 12 well plate at a seeding density of 40.000 cells/well. As previously described, cells were starved, treated with LXA4 and activated with TGF-β for 24 h. Next, the cells were washed 3 times with serum-free medium. After 48 h of incubation with serum-free medium the medium was collected for use in conditioned medium experiments.

Table 1
Sequences of forward and reverse primers used during real-time PCR.

Gene	Forward Primer	Reverse Primer
RPS18	TGAGGTGGAACGTGTGATCA	CCTCTATGGGCCCGAATCTT
Acta-2 (α-SMA)	CCCCATCTATGAGGGCTATG	CAGTGGCCATCTCATTTTCA
Collagen1α1	GTACTGGATTGACCCCAACC	CGCCATACTCGAACTGGAAT
Collagen3α1	AAGAAGGCCCTGAAGCTGAT	GTGTTTCGTGCAACCATCCT
PDGFβR	AGGCAAGCTGGTCAAGATCT	GCTGTTGAAGATGCTCTCCG
MMP2	AGGAGGAGAAGGCTGTGTTC	CTCCAGTTAAAGGCGGCATC
WNT2β	TTTAGGTGCTGGTGGGAGAG	CTCTTCTTCACCTGGGAGCA
IDI1	TTGGGCTGGATAAAACCCCT	GCAACATCCGGCATAACTGT
NSDHL	ATGCTATGGAGAGGACCGTG	CAGAAGGAGTCACAGGCTCA
INSIG1	GGCAGCTTCCCAAGTATTCG	CTACCTCCTTTGGGCACTGA
CXCL12	TGCCCTTCAGATTGTAGCCC	GCGTCTGACCCTCTCACATC
CTGF	GTTTGGCCCAGACCCAACTA	GGCTCTGCTTCTCTAGCCTG

2.7. Cell proliferation assay

hPSCs were seeded into a 96 well plate at a density of 2.500 cells/well. The next day, hPSCs were treated with 10 nM of LXA4. Cell number was monitored every 24 h over a time period of 72 h. To monitor the cell number, 10 μl of Alamar Blue dye (Invitrogen, Carlsbad, USA) in 100 μl of hPSC growth media was added per well. After 4 h the fluorescent signal was measured using a VIKTOR™ plate reader (Perkin Elmer, Waltham, Massachusetts). To evaluate the effect of hPSC conditioned media on Panc-1 and AsPc-1 cell growth, Panc-1 and AsPc-1 were seeded in a 96 well plate at a density of 5000 cells/well. 24 h after seeding the previously collected condition media was applied to the cells. Cell number was monitored at 0 h, 24 h and 48 h as described previously.

2.8. Wound healing assay

To evaluate the effect of LXA4 on hPSC migration, cells were seeded into a 24 well plate at a seeding density of 50.000 cells/well. As previously described cells were starved, treated with LXA4 and activated with TGF-β for 24 h. A scratch was made on the culture plate using a 200 μl pipette tip fixed in a custom-made holder. Next, cells were washed and incubated with fresh serum-free media. Images were captured at $t = 0$ h and $t = 12$ h, with an EVOS microscope. Images were analysed by Image J software to calculate the area of the scratch and represented as percentage of wound closure.

2.9. Transwell migration assay

To evaluate the effect of hPSC conditioned media on Panc-1 and AsPc-1 migration, Panc-1 and AsPc-1 were seeded into the upper chamber of a 24 well Transwell insert (Sigma Aldrich) at a seeding density of 50.000 cells/well. After 24 h, the cells were fixed with ice cold methanol (Fisher Scientific) for 10 min. Next, the cells were incubated with 0.1% Crystal Violet solution (Sigma Aldrich) in 25% methanol (Fisher Scientific) for 10 min. After washing the cells with MilliQ water, cells from the upper compartment were removed with a cotton swap and the inserts were allowed to dry. The migrated cells were imaged with a Nikon microscope (Nikon Eclipse E400, Tokyo, Japan). Images were analysed by Image J software to calculate the positively stained area.

2.10. Spheroid formation assay

3D-heterospheroids containing a mixture of hPSCs and Panc-1 cells were prepared using the hanging drop method. hPSCs and Panc-1 were trypsinized and suspended in their respective culture medium to a concentration of 300.000 cells/ml. The hPSCs and Panc-1 cell suspensions were mixed 1:1 (v/v). For spheroid formation, a drop of 20 μl containing 6000 cells were dispensed onto a lid of a round bottom suspension culture 96-well plate (Greiner BioOne, Alphen aan den Rijn, The Netherlands). Next, the lid was inverted and placed onto the 96-well plate. Wells were filled with 150 μl PBS for humidity. For spheroids prepared with LXA4-treated hPSCs, hPSCs were seeded, starved for 24 h and treated with 10 nM LXA4 for an additional 24h. The spheroids were grown for eight days. Spheroids which were LXA4-treated after formation were allowed to form for 4 days. Next, 10 μl of 20 nM LXA4 was directly added into the droplet. The spheroids were grown for an additional 8 days. Spheroids were imaged under an inverted microscope, and their area was measured digitally using ImageJ software.

2.11. Immunohistochemical staining of 3D-heterosperoids

For sectioning 3D-heterospheroids were collected, embedded in

Cryomatrix (Thermo Scientific) and frozen at - 80 °C. Afterwards, spheroids were cut into 6 μm thick sections using a Cryotome FSE (Thermo Scientific). The spheroids collected on microscope slides were rehydrated in PBS for 5 min before fixation in 4% paraformaldehyde (Sigma Aldrich) for 30 min. Next, the slides were washed 3 times with PBS (5 min each). The edges of the slides were marked with a hydrophobic Pap-pen (Life Technologies). After washing, the cells were permeabilized with 0.1 vol % Triton-X (Sigma Aldrich) in PBS for 15 min and washed again. Slides were incubated with the primary antibody (Supplementary Table 2) diluted in PBS overnight at 4 °C. The next day, the slides were washed 3 times with PBS before the secondary fluorescent antibody (see Supplementary Table 2) diluted in PBS supplemented with 5 vol% of normal human serum (Thermofisher Scientific) were added. Finally, the slides were washed and mounted with fluoroshieldTM with DAPI (Sigma Aldrich) for staining of nuclei. Sections have been imaged using a Hamamatsu NanoZoomer Digital slide scanner 2.0HT (Hamamatsu Photonics, Bridgewater NJ).

2.12. Animal study

Six-week-old male CB17 SCID mice (Janvier Labs, Le Genest-Saint-Isle, France) were subcutaneously injected with a mixture of 2×10^6 Panc-1 and 4×10^6 of hPSCs. Tumor formations and volumes were assessed every 3–4 days. Tumor volumes were calculated using a standard formula (volume = length × width^2). The treatment was started 9 days after injection of the tumors. Six tumor-bearing mice per treatment groups were taken and injected with either vehicle or LXA4 twice a week. Of each group half were injected intraperitoneal (40 μg/kg) and another half local intratumoral (4 μg/kg). At the end of the experiments, animals were sacrificed under anesthesia, tumors were harvested and immediately snap frozen in cold 2-methyl butane (Fisher Scientific). Frozen tumors were stored at −80 °C until analysis.

2.13. Immunohistochemical staining of mouse tumors

Mouse tumors were embedded in Cryomatrix (Thermo Scientific) and frozen at - 80 °C. Afterwards, spheroids were cut into 6 μm thick sections using a Cryotome FSE (Thermo Scientific). The tumor section were dried and fixed in acetone (Fisher Scientific) for 10 min. The edges of the slides were marked with a hydrophobic Pap-pen (Life Technologies). Next, the tumor sections were rehydrated in PBS for 10 min. Tumor sections were incubated with the primary antibody (Supplementary Table 2) diluted in PBS overnight at 4 °C. The next day, the slides were washed 3 times with PBS before the secondary fluorescent antibody or HRP-labeled antibody (Supplementary Table 2) diluted in PBS supplemented with 5 vol% of normal mouse serum (Thermofisher Scientific) were added (normal human serum was used for α-SMA staining). Staining with HRP-labeled secondary antibodies was continued as described elsewhere [27]. For staining with fluorescent antibodies, the slides were washed and mounted with fluoroshieldTM with DAPI (Sigma Aldrich) for staining of nuclei. Sections have been imaged using a Hamamatsu NanoZoomer Digital slide scanner 2.0HT (Hamamatsu Photonics, Bridgewater NJ).

2.14. Immunohistochemical staining of human tumors

Human paraffin embedded PDAC sections were deparaffinized in xylene, rehydrated in serially diluted alcohol solutions, followed by demineralized water. Antigen retrieval was performed by at 80 °C using Tris buffer (pH 9.0, Dako, Glastrup, Denmark) for 16 h. To block endogenous peroxidase, slides were incubated in 0.3% hydrogen peroxide in phosphate-buffered saline (PBS) for 20 min. Next, slides were incubated for 2 h with an antibody against α-SMA (A2547 Sigma, the Netherlands), followed by incubation with the secondary antibody for 60 min at room temperature. The immunohistochemical staining was visualised using 3.3-diaminobenzidine tetrahydrochloride solution (Dako) for 5–10 min resulting in a brown staining and then counterstained with hematoxylin, dehydrated and finally mounted in vectamount.

2.15. Graphs & statistical analysis

All graphs were made using GraphPad Prism Vol.5 (GraphPad Software Inc., San Diego, CA). All values are expressed as a mean ± standard error of the mean (SEM). Statistical significance of the results was performed by either a two-tailed unpaired student's t-test for comparison of two treatment groups or a one-way ANOVA to compare multiple treatment groups. Differences were considered significant for a p-value of $^*p < 0.05$, $^{**}p < 0.01$, $^{***}p < 0.001$, respectively.

3. Results

3.1. LXA4 expression is induced in TGF-β activated hPSCs

LXA4 binds to the extracellular domain of the N-formyl-peptide receptor 2 (FPR2) receptor as shown in Fig. 1 A. To achieve the effect of LXA4 on hPSCs, it is crucial to confirm whether these cells express the FPR2 receptor in their quiescent and active state. Therefore, we activated hPSCs with TGF-β for 48 h and examined the protein expression of FPR2 using western blot analysis. As shown in Fig. 1 B, the expression of FPR2 receptor was induced by about 6.5-fold in the TGF-β-activated hPSCs compared to the non-activated form (Fig. 1 B, C). To confirm the activation of hPSCs with TGF-β we have performed a western blot for α-SMA, showing the significant induction of this CAF marker upon TGF-β treatment (Fig. 1 B, D).

3.2. LXA4 inhibits TGF-β induced hPSC differentiation

As shown in Fig. 2A and D, after activation with TGF-β, hPSCs attained a myofibroblast phenotype, as can be seen with their high expression of α-SMA and collagen1 (Col1) and stretched morphology. Treatment with LXA4 not only significantly inhibited the protein expression of α-SMA and Col1 in a concentration dependent manner, but also inhibited the change in the morphology (Fig. 2 A, D). The quantitation of stainings confirmed the reduction in the expression of both α-SMA and Col1 with the most profound effects at a concentration of 10 nM (Fig. 2 B, C). Interestingly, LXA4 at 10 nM concentration significantly inhibited the TGF-β-induced expression of genes encoding for the CAF phenotype, including growth factors (CTGF and CXCL12), membrane receptors (PDGFβR), cytokines inducing cancer cell growth (IL-6), enzymes facilitating increased ECM turnover and altered ECM deposition (MMP2), genes involved in cholesterol production and homeostasis (IDI1, INSIG1, NSDHL), intracellular proteins (Acta-2 (encoding for α-SMA), Wnt2B) and ECM proteins (Col1α1, Col3α1) (Fig. 3 A). Additionally, we detected a significant reduction in TGF-β-induced expression of secreted MMP-2 in the conditioned medium of hPSCs treated with 10 nM of LXA4 (Supplementary Fig. 2). Of note, treatment of hPSCs with 10 nM LXA4 over a period of 72 h exerted no toxic effects on their metabolic activity (Fig. 3 B). Next, we examined the effect of LXA4 on the migration of hPSCs using a scratch (wound healing) assay. The migration potential in TGF-β-activated hPSCs was not induced compared to untreated hPSCs (Fig. 3 C). LXA4 led to a significant inhibition of the wound closure in both non-activated and TGF-β-activated hPSCs compared to

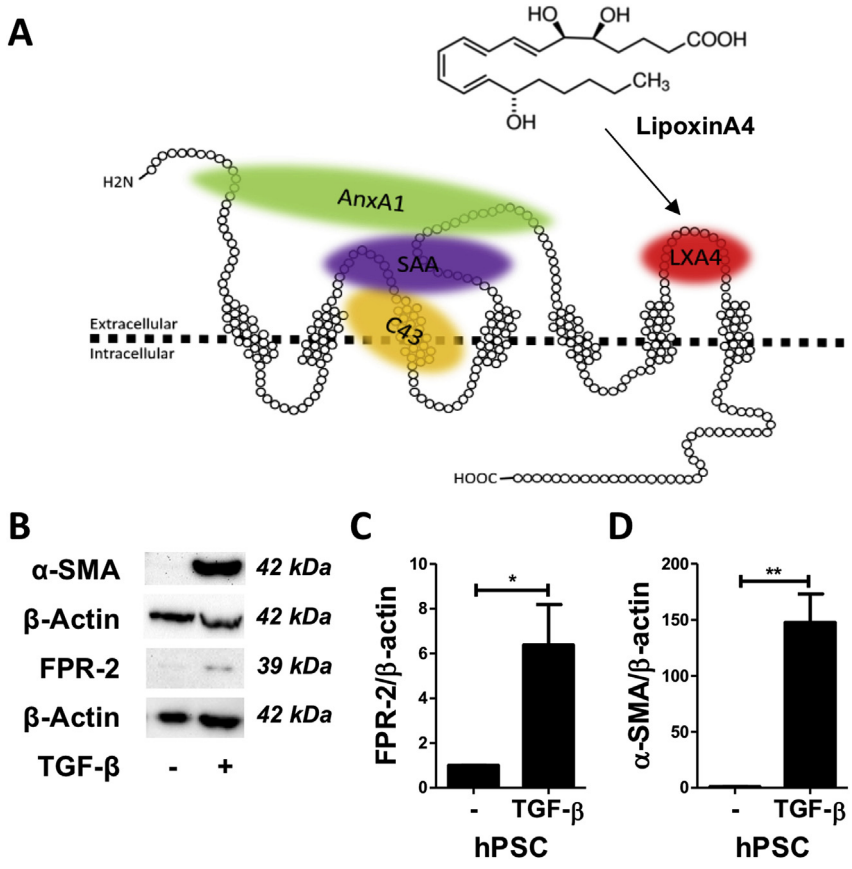

Fig. 1. Structure and protein expression of the Lipoxin A4 (LXA4) specific surface receptor FPR2 on hPSCs. Structure of the LXA4-specific surface receptor FPR2 displaying the binding site of LXA4 (**A**). Protein expression of the LXA4-specific surface receptor FPR2 (**B, C**) and the activation marker α-SMA (**B, D**) in hPSCs and hPSCs activated with TGF-β for 48 h (**B**). Data represents mean ± SEM for at least 3 independent experiments. Statistical analysis was performed by two-tailed unpaired student t-test. Statistical differences are $^{*}p < 0.05$, $^{**}p < 0.01$.

control cells (Fig. 3 C). These data indicate that LXA4 inhibits the activation of hPSCs with TGF-β to attain the CAF-like myofibroblast phenotype.

3.4. LXA4 inhibits TGF-β induced smad 2/3 nuclear translocation and phosphorylation

Since LXA4 inhibited the TGF-β-mediated activation of hPSCs, we examined the effect of LXA4 on the TGF-β signalling pathway. After binding to its receptor, TGF-β activates the Smad 2/3 pathway, whereby Smad 2/3 gets phosphorylated and locates within the nucleus. As shown in Fig. 4 A using immunofluorescent microscopy, in non-activated hPSCs, Smad2/3 was localized in the cytoplasm but not in the nuclei, while after 30 min incubation with TGF-β, Smad 2/3 translocated into the nuclei (Fig. 4 A). Treatment with LXA4 reduced the translocation into the nuclei (Fig. 4 A). To confirm the activation state of Smad2/3 and quantify this, we examined the phosphorylated Smad2/3 (pSmad2/3) using immunofluorescent staining which clearly showed a significant translocation of pSmad2/3 into the nuclei of hPSCs upon TGF-β activation compared to untreated cells (Fig. 4 A). Importantly, the nuclear translocation of pSmad 2/3 was significantly inhibited by LXA4, as shown in the immunofluorescent pictures and quantitative data (Fig. 4 A, B). Additionally, we have performed a Western Blot to analyse the protein expression of Smad 2/3 and pSmad 2/3 (Supplementary Figure 1 A) and found a significant reduction in the pSmad 2/3/ Smad 2/3 ratio (Supplementary Figure 1 B), confirming the inhibition of Smad 2/3 phosphorylation, which we previously had observed in immunofluorescent staining.

3.5. LXA4 inhibits hPSC-mediated paracrine effects on tumor cells

After confirming the direct effect of LXA4 on hPSCs, we investigated the hPSC-induced paracrine effect on the growth and migration potential of human pancreatic tumor cells (Panc-1 & AsPc-1). To study that, we collected conditioned media from hPSCs with or without activation with TGF-β to collect hPSC-secreted cytokines and growth factors (Fig. 5 A). Incubation of Panc-1 cells with the conditioned media from TGF-β-activated hPSCs showed an induced Panc-1 cell growth and migration compared to the conditioned media from non-activated hPSCs (Fig. 5 B, C). Interestingly, conditioned media collected from LXA4-treated hPSCs showed reduced Panc-1 cell growth and migration (Fig. 5 B, C). For AsPc-1 tumor cells we observed the same trend, with regard to their migration and cell growth, in LXA4-treated hPSCs (Supplementary Fig. 3 A, B) (Supplementary Figure 3 D). Next, we wanted to study the effect of LXA4 on hPSCs in direct contact of Panc-1 cells using a 3D-heterospheroid co-culture system, as shown earlier by us elsewhere [28]. In order to investigate the effect of LXA4 on 3D-heterospheroid formation and growth, we formed spheroids with hPSC that were treated with LXA4 prior to the experiment (Fig. 5 E). Properly formed spheroids were imaged 8 days after formation using bright-field microscopy and measured for their size (Fig. 5 F). The results showed a significant reduction in spheroid size when hPSCs were treated with LXA4 before spheroid formation when compared to spheroids formed with EtOH-treated

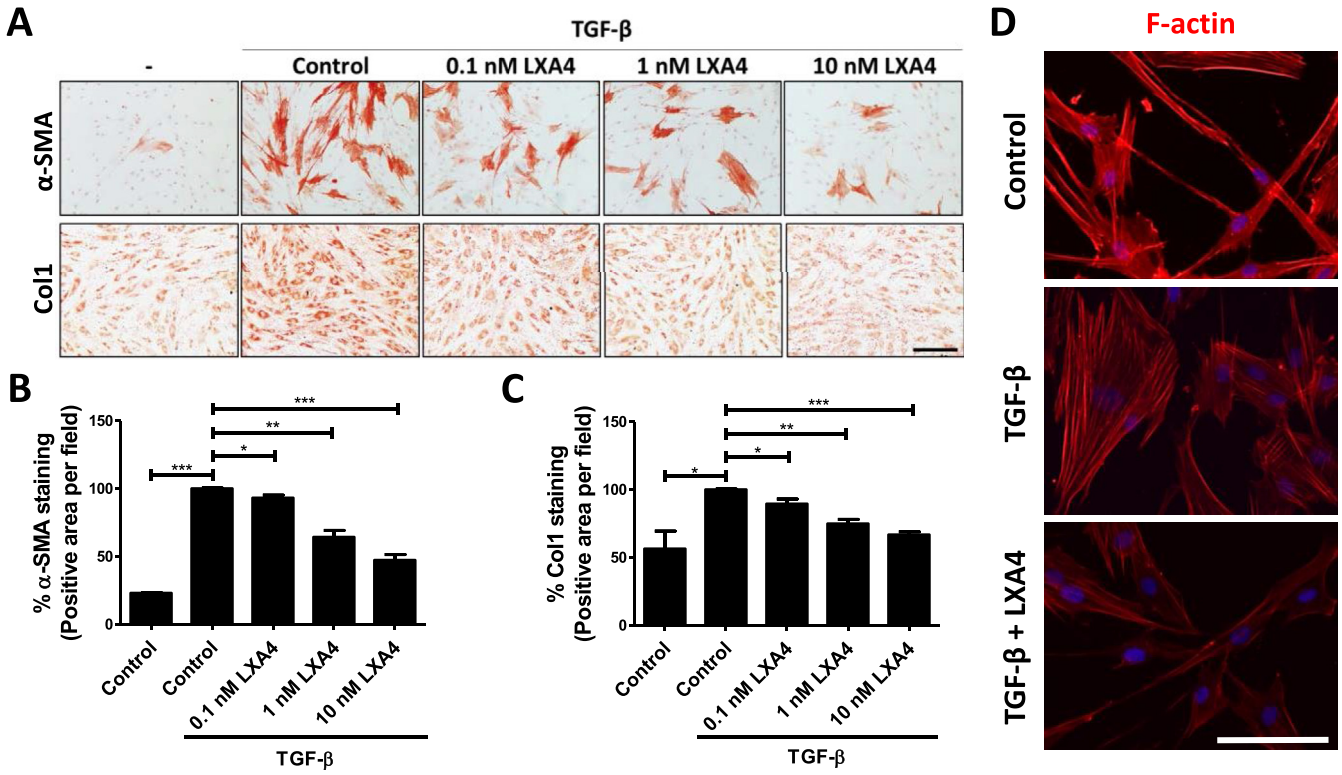

Fig. 2. Lipoxin A4 effect on TGF-β mediated hPSC differentiation. Immunostaining showing the inhibitory effect of LXA4 (0.1, 1, 10 nM) on the protein expression of α-SMA and Col1 (**A**). Scale bar = 200 μm. Quantification of α-SMA (**B**) and Col1 (**C**) staining for the respective concentrations of LXA4. F-actin staining showing morphological changes in TGF-β activated and LXA4-treated and TGF-β activated compared to normal hPSCs (**D**). Control contains 0.001% ethanol. Data represent mean + - SEM for at least 3 independent experiments. Statistical analysis was performed by two-tailed unpaired student t-test. *p < 0.05, **p < 0.01, ***p < 0.001.

hPSCs (Fig. 5 E). Strikingly, spheroids formed with LXA4-treated hPSCs were not yet formed at day 4 after the initiation of spheroid formation, while spheroids containing EtOH-treated hPSCs had already formed (Fig. 5 G). After 8 days the rate of 3D-heterospheroid formation was ~80% for spheroids formed with EtOH-treated hPSCs and ~15% for spheroids formed with LXA4-treated hPSCs (Fig. 5 G). To investigate whether LXA4 does also inhibit hPSC activation in 3D-heteropheroids, we performed immunofluorescent staining on 6 μm thick sections of hPSC/Panc-1 3D-heterospheroids (Fig. 5 H). We found that spheroids formed with LXA4-treated hPSCs expressed significantly lower levels of Col1 compared to EtOH-treated hPSCs (Fig. 5 H, I). These data signify that LXA4 intervenes into the crosstalk between hPSCs and tumor cells by inhibiting the activation of hPSCs.

3.6. *LXA4 inhibits the growth of hPSC/Panc-1 3D-heterospheroids*

To investigate whether LXA4 also exerts an inhibitory effect on hPSC/Panc-1 3D-heterospheroid growth, we treated the established spheroids (4 days) with either EtOH or LXA4 and followed their growth. Similar to an *in vivo* tumor model, this 3D model involved the treatment after tumor a formation. The spheroids growth was observed over a time period of 12 days. A significant difference in spheroid growth between the LXA4 and control treated group was observed 2 days after the start of the treatment (Fig. 6 A, B). Furthermore, the control treated spheroids showed newly formed areas of proliferating cells on their surface, which was not observed in LXA4 treated spheroids (Fig. 6 A). In addition, we examined the effect of LXA4 on the spheroids solely consisting of Panc-1 cells to investigate if LXA4 also inhibits the Panc-1 3D-spheroid growth (Fig. 6 C). No significant decrease in spheroid growth could be observed in the LXA4-treated in comparison to the control Panc-1 3D-spheroids (Fig. 6 C). To examine the effect of LXA4 on the activation of hPSCs, we performed immunofluorescent staining on 3D-heterospheroids at day 12. Interestingly, significantly decreased levels of Col1 (Fig. 6 E, F) were found in LXA4-treated compared to EtOH-treated 3D-hetrospheroids. These data indicate that the reduction in the growth of the 3D-heterospheroids is due to inhibition of hPSC activation and its tumor-inducing effect but not due to a direct effect on the tumor cells.

3.7. *LXA4 inhibits in vivo subcutaneous tumor growth and collagen deposition in mice*

To investigate the effect of LXA4 on *in vivo* tumor growth we co-injected hPSCs and Panc-1 into the flank of immunodeficient mice (Fig. 7 A). These tumors are rich in α-SMA and thereby mimic the microenvironment of human PDAC patients (Supplementary Fig. 5). After the tumors were established, we treated the mice with either intratumoral (IT, 4 μg/kg) or intraperitoneal (IP, 40 μg/kg) injections of LXA4 or EtOH, twice a week (Fig. 7 B). Both, IT and IP injections of LXA4 significantly inhibited the tumor growth compared to control animals, immediately after the treatment (Fig. 7 B). The difference in tumor size of EtOH-treated and LXA4-treated animals stayed significant until the mice were sacrificed on day 31 after the first injection (Fig. 7 B). LXA-4 treatment showed no significant effects on the body weight of subcutaneous tumor bearing mice (Fig. 7 C). Immunofluorescent staining showed a significant reduction (~60%) of Col1 in both IT and IP treated tumors compared to control tumors (Fig. 7 D, E). Additional stainings for the CAF marker (α-SMA), blood vessel marker (endothelial marker, CD31) did not show significant differences between EtOH- and LXA4-treated tumors, but there was

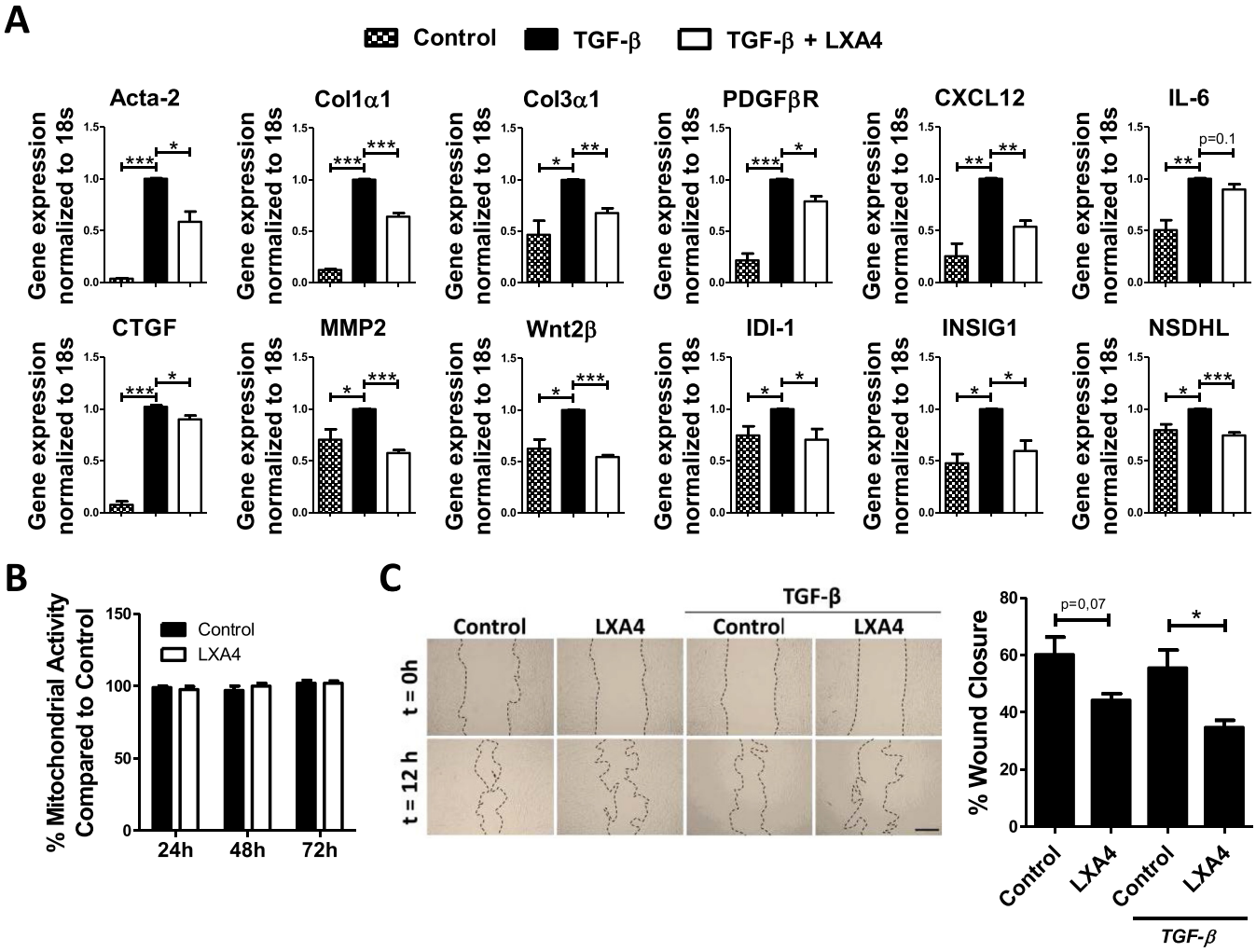

Fig. 3. Lipoxin A4 effect on TGF-β mediated hPSC differentiation, viability and migration potential. Gene expression of hPSC activation markers encoding growth factors (CTGF), membrane receptors (PDGFβR), chemokines (IL-6 and CXCL12), enzymes (MMP2), proteins involved in cholesterol production and homeostasis (IDI1, INSIG1 and NSDHL), intracellular proteins (α-SMA, Wnt2β) and ECM proteins (Col1α1, Col3α1) displaying the inhibitory effect of 10 nM LXA4 after treatment with 5 ng/ml TGF-β LXA4 (**A**). Mitochondrial activity of hPSCs treated with 10 nM Lipoxin A4 and EtOH control after 24, 48 and 72 h of incubation (**B**). Representative microscopic images and quantification showing the effect of LXA4 (10 nM) on the migration of hPSCs and hPSCs activated with TGF-β (**C**). Scale bar = 500 μm. Control contains 0.001% ethanol. Data represent mean + - SEM for at least 3 independent experiments. Statistical analysis was performed by two-tailed unpaired student t-test. $^{*}p < 0.05$, $^{**}p < 0.01$, $^{***}p < 0.001$.

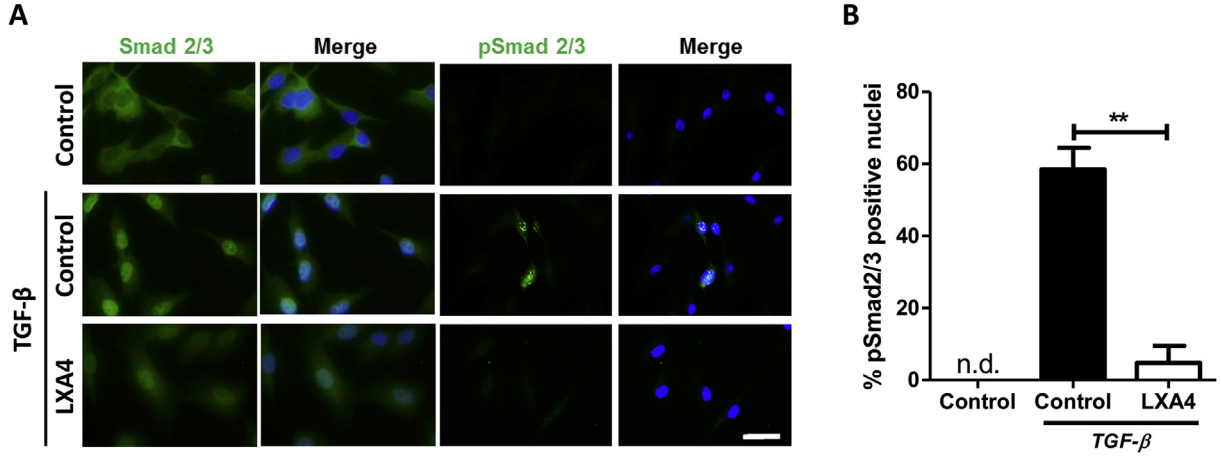

Fig. 4. Effect of LXA4 on Smad 2/3 phosphorylation in TGF-β activated hPSCs. Immunofluorescent staining of Smad 2/3 and pSmad 2/3 in hPSCs, TGF-β activated hPSCs treated with control or 10 nM LXA4 (**A**). Scale bar = 50 μm. Quantification of fluorescent pSmad 2/3 staining showing the percentage of pSmad 2/3 positive nuclei (**B**). Control contains 0.001% ethanol. Data represent mean + SEM for at least 3 independent experiments. Statistical analysis was performed by two-tailed unpaired student t-test. $^{**}p < 0.01$.

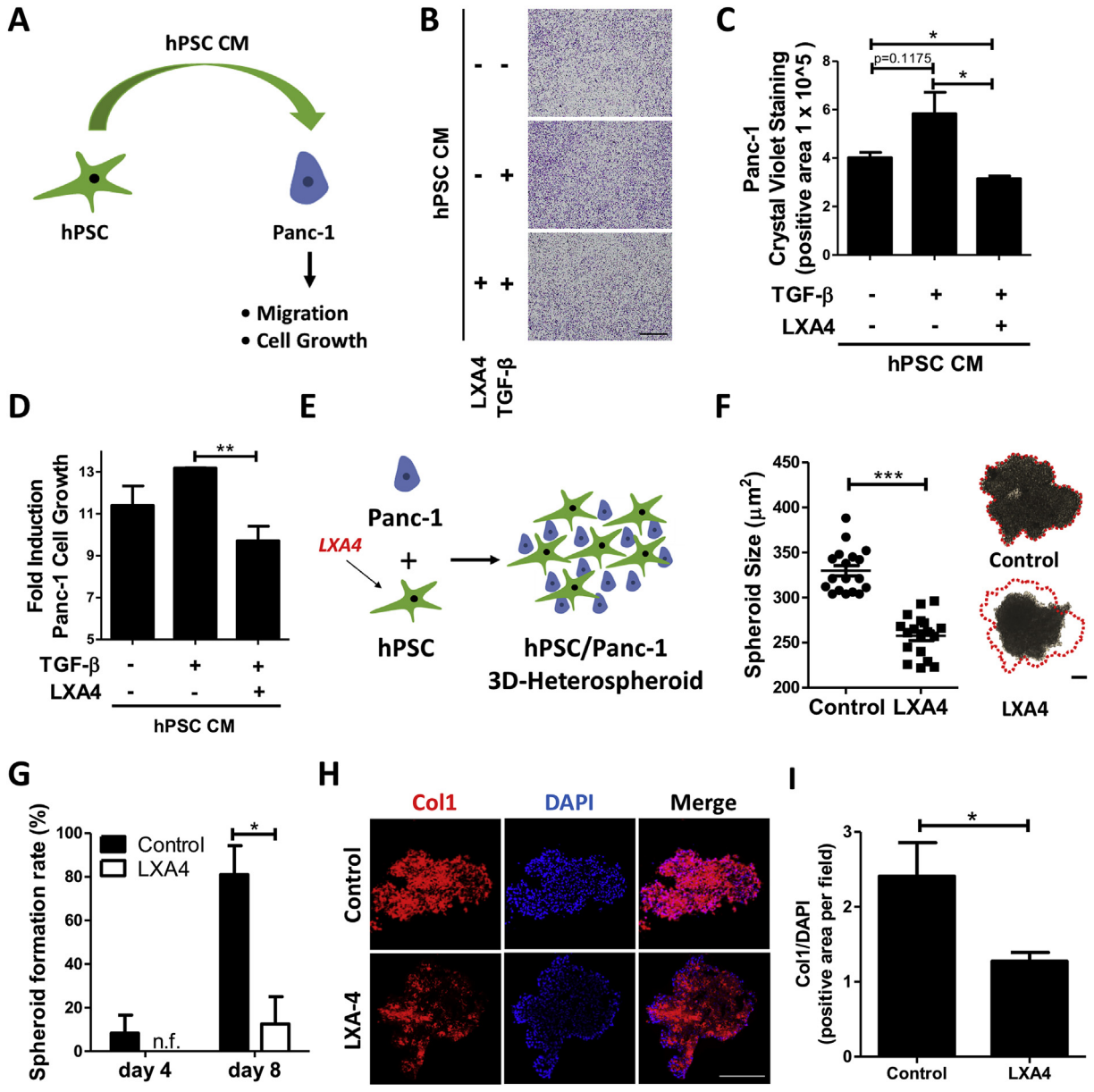

Fig. 5. Effect of LXA4 on hPSC-induced tumor cell migration, proliferation and 3D-heterospheroid formation. Schematic representation of the hPSC conditioned medium experiment (**A**). Representative images (**B**) and quantification (**C**) of Panc-1 tumor cell migration after 24 h of incubation with condition medium collected from untreated, control-treated TGF-β activated hPSCs and 10 nM LXA4-treated TGF-β activated hPSCs. Scale bar = 400 μm. Panc-1 epithelial tumor cell growth after 48 h of incubation with condition medium collected from untreated, control-treated TGF-β activated hPSCs and 10 nM LXA4-treated TGF-β activated hPSCs (**D**). Schematic representation of spheroid formation (**E**). Size of hPSC/Panc-1 3D-heterospheroid formed with control-treated or LXA4-treated hPSCs after 8 days, including representative images of hPSC/Panc-1 3D-heterospheroids formed with control-treated of LXA4-treated hPSCs (**F**). Scale bar = 100 μm. Formation rate in percent of hPSC/Panc-1 3D-heterospheroid formed with control-treated of LXA4-treated hPSCs after 4 and 8 days (**G**). Immunofluorescent staining on 6 μm thick sections of hPSC/Panc-1 3D-heterospheroid formed with control-treated of LXA4-treated hPSCs for the expression Col1 and nuclei staining (DAPI) (**H**). Scale bar = 200 μm. Quantification of Col1 staining divided by DAPI staining of hPSC/Panc-1 3D-heterospheroid formed with control-treated of LXA4-treated hPSCs (**I**). Control contains 0.001% ethanol. Data represent mean + SEM for at least 3 independent experiments. Statistical analysis was performed by two-tailed unpaired student t-test. $^{*}p < 0.05$, $^{**}p < 0.01$, $^{***}p < 0.001$.

a trend showing the reduction of these markers with LXA4 treatment (Supplementary Fig. 4).

4. Discussion

The abundant desmoplastic reaction in PDAC, also known as pancreatic tumor stroma, plays an important role in cancer progression, invasion, metastasis and response to therapy [4]. Reprogramming of the tumor stroma by dampening the function of hPSCs would be an interesting approach to gain therapeutic benefits for the treatment of cancer. In earlier studies, a natural biomolecule vitamin D has been shown to reverse hPSC activation to improve drug delivery efficiency and prolong survival in animals [5]. In this study, we explored the therapeutic potential of a highly potent endogenous lipid mediator, LXA4, for the treatment of pancreatic tumors. We showed that LXA4 inhibited the activation of hPSCs into CAF-like myofibroblasts in vitro and thereby inhibited hPSC-induced tumor-promoting effects. In our novel 3D-heterospheroidal co-cultures, LXA4 could inhibit the activation of hPSCs within the 3D microenvironment and reduced spheroid growth.

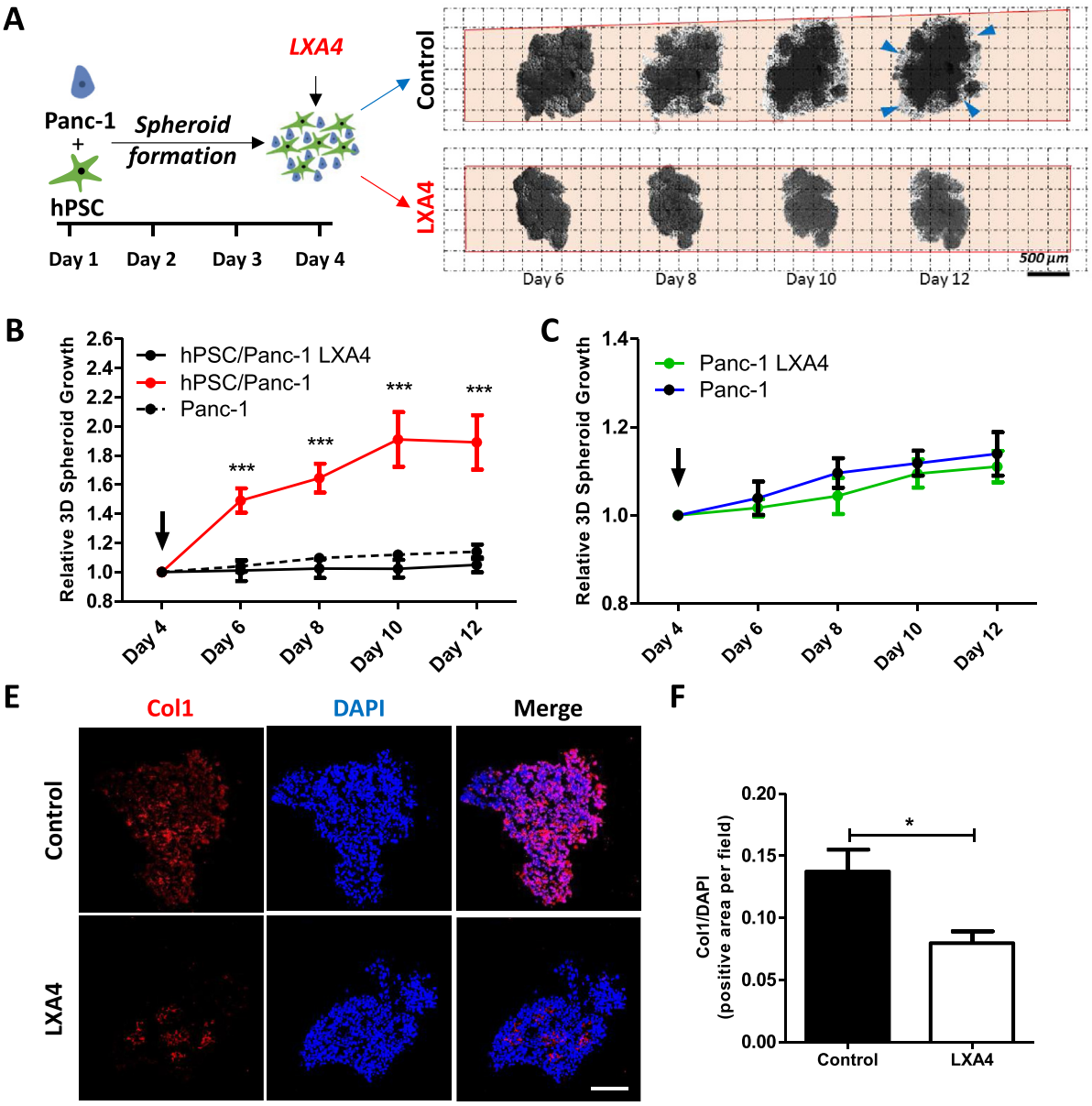

Fig. 6. Effect of LXA4 on hPSC/Panc-1 spheroid growth. Representative images (**A**) and quantification (**B**) of hPSC/Panc-1 3D-heterospheroid growth after treatment with LXA4 or control and Panc-1 3D-heterospheroids 4 days after initiation of the experiment. Black arrow indicates treatment with LXA4 or control, blue arrows indicate proliferating cells. Growth of Panc-1 3D-spheroids after treatment with LXA4 compared to control treated spheroids (**C**). Immunofluorescent staining (**E**) and quantification for the expression of Col1 (**F**) and nuclei staining (DAPI) (**F**) in 6 µm thick section of control and LXA4 treated 3D-heterospheroids after 12 days of spheroid formation. Control contains 0.001% ethanol. Data represent mean + SEM for at least 3 independent experiments. Statistical analysis was performed by two-tailed unpaired student t-test. *p < 0.05, **p < 0.01, ***p < 0.001. (For interpretation of the references to colour in this figure legend, the reader is referred to the Web version of this article.)

Finally, we showed the therapeutic efficacy of LXA4 in vivo in a co-injection tumor model. This study highlights LXA4 as an interesting biological to be developed for the treatment of pancreatic cancer.

Human PSCs are regarded as the main source of CAFs in the stroma of pancreatic cancer [12] and as response to activation with TGF-β they acquire a CAF-like myofibroblast phenotype, as shown previously by us and others [29–31]. LXA4 a highly potent endogenous lipid is known for its anti-inflammatory function and has been shown to inhibit fibrosis in renal mesangial cells, human lung (myo)fibroblasts and experimental renal fibrosis [13,23,24]. Here we show that the LXA4-specific surface receptor FPR2 is expressed in hPSCs and highly upregulated in myofibroblast-like activated hPSCs. This result demonstrates that activated hPSCs present a valid target for treatment with LXA4. Our work illustrates for the first time that LXA4 treatment reduces the expression of fibrosis related myofibroblast markers α-SMA and Col1 in TGF-β activated hPSCs in vitro, which was accompanied by a reversal of the elongated, stretched myofibroblast-like phenotype of those cells into their normal phenotype. In addition, LXA4 treatment significantly reduced the TGF-β-induced expression of α-SMA, Col1α1, Col3α1, PDGFRβ, MMP2, Wnt2B, NSDHL, CXCL12, IL,6, CTGF, IDI1 and INSIG1, all markers which were previously found to be induced in activated PSCs by transcriptome analysis [5,32]. Of special significance are the LXA4 targets Col1α1 and Col3α1 of the extracellular matrix, limiting chemotherapeutic activity by blocking drug delivery [33,34], and growth factors CTGF and CXCL12,

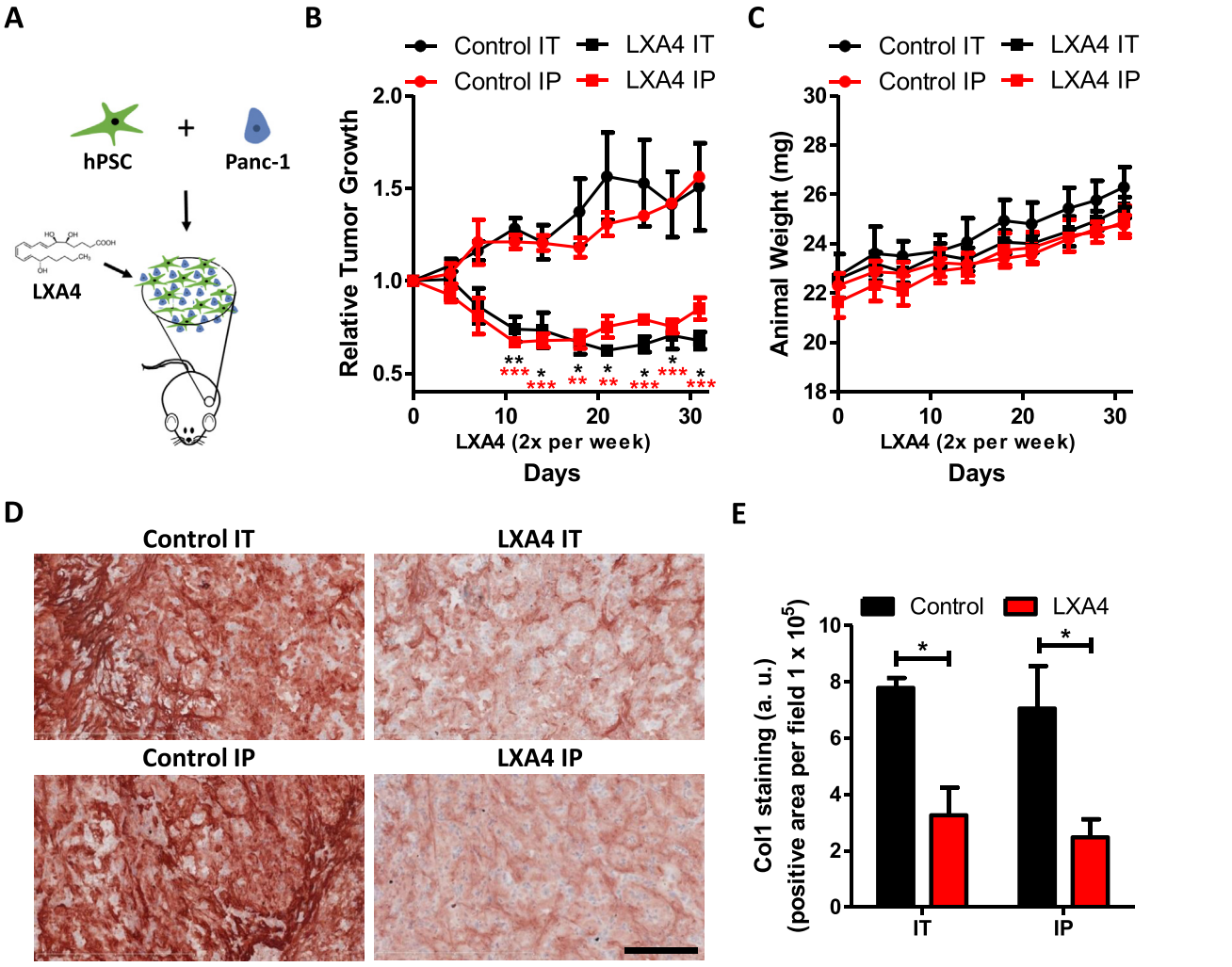

Fig. 7. Effect of LXA4-treatment on *in vivo* tumor growth and Col1 expression of Panc-1/PSC subcutaneous tumors in mice. Schematic representation of the co-injection (Panc-1 and hPSCs) subcutaneous tumor model (**A**). The effect of intra tumoral (IT) and intra peritoneal (IP) injection of LXA4 on the tumor growth of co-injection (Panc-1 + PSCs) subcutaneous xenografts in mice (**B**). Arrow indicate times of injection. The effect of intra tumoral (IT) and intra peritoneal (IP) injection of LXA4 on the body weight of co-injection (Panc-1 + PSCs) subcutaneous xenograft bearing mice (**C**). Immunostaining (**D**) and quantification (**E**) of staining for Col1 in tumors treated IT and IP with LXA4. Scale bar = 200 μm. Control contains 0.001% ethanol. Data represent mean ± SEM for at least 3 independent experiments. *p < 0.05, **p < 0.01, ***p < 0.001.

known to potentiate the tumor response to gemcitabine [35] and restore T-cell response [36], respectively. The effects of LXA4 on transcriptional changes in hPSCs were supported by a reduction in hPSC migration upon LXA4 treatment, confirming the significance of LXA4 in controlling hPSC's phenotypic behaviour. These findings illustrate that LXA4 treatment remodels activated hPSCs into their quiescent state by transcriptional remodelling and thereby inhibits the capacity of those cells to support pancreatic tumor growth. Upon activation of hPSCs with TGF-β the Smad 2/3 signalling pathway is activated, resulting in phosphorylation of the Smad 2/3 protein [37]. This data demonstrates that TGF-β induced transcriptional and phenotypic changes were controlled by LXA4-induced inhibition of Smad 2/3 phosphorylation, which has earlier been observed by Börgeson et al. in renal rat fibroblasts [38]. Previous studies have demonstrated that hPSCs can induce tumor-promoting paracrine effects by secreting mutagenic factors such as growth factors and cytokines to induce tumor progression, invasion and metastasis [39,40]. Interestingly, our study shows a modulation of the secretory phenotype of hPSCs after treatment with LXA4, which attenuated hPSC-mediated cell growth and migration of Panc-1 and AsPc-1 tumor cells. These results are in line with previous studies in which hPSCs paracrine effects on tumor cells were reduced by the means of microRNA [29]. The inhibitory effect of LXA4 on hPSC activation and hPSC induced tumor promoting effects were not only limited to 2D cell cultures but also inhibited the formation, growth and ECM-deposition of 3D-heterospheroids formed from hPSCs and Panc-1. These 3D-heterospheroids provide tumor-like characteristics such as a dense, hypoxic core, ECM production and direct crosstalk between stromal and cancer cells. In line with our *in vitro* data, administration of LXA4 via IT or IP injection into hPSC/Panc-1 subcutaneous tumors in mice reduced Col1 deposition, the major ECM protein within the pancreatic tumor stroma. Finally, the reduced ECM deposition within these tumors, resulted in attenuated tumor progression. In this context, it is important to point out, that ECM degradation resulting in improved intratumoral blood flow and drug delivery has shown survival benefits in pancreatic cancer [6,41]. Staining for the CAF marker αSMA was reduced in the tumors of mice which obtained IP injections of LXA4 but not in IT treated tumors (Supplementary Figure 4 A), indicating normalization of the CAF phenotype. The reduced α-SMA expression in only IP treated mice points out towards the additional systemic effect of LXA4. However, since the

local IT injection reduced the tumor growth, it is clear that the tumor-inhibitory effect of LXA4 is due to a direct effect on the tumor stroma. In addition, LXA4 reduced angiogenesis, a key tumor-promoting mechanism, in tumors of both IT and IP LXA4-treated animals, indicated by the endothelial marker CD31 (Supplementary Figure 4 B).

In conclusion, this study demonstrated for the first time that LXA4 is capable to attenuate tumor growth by inhibiting PSC-induced desmoplasia in pancreatic tumors, by reversing hPSC activation into CAF and modulating hPSC induced tumor promoting effects. Therefore, LXA4 is a potential candidate to be evaluated for the treatment of pancreatic tumor and for its potential to increase the efficacy of chemo- and radiotherapy.

Financial supports

The study was supported by the Swedish Research Council, Stockholm (project no. 2011-5389) and the MIRA Institue for Biomedical Technology and Technical Medicine, University of Twente, The Netherlands.

Conflicts of interest

J Prakash is a founder and stakeholder of ScarTec Therapeutics BV. Enschede. The authors have no other relevant affiliations or financial involvement with any organization or entity with a financial interest in or financial conflict with the subject matter or materials discussed in the manuscript apart from those disclosed.

Appendix A. Supplementary data

Supplementary data related to this article can be found at https://doi.org/10.1016/j.canlet.2018.01.072.

References

[1] R.L. Siegel, K.D. Miller, A. Jemal, Cancer statistics, 2016, CA Canc. J. Clin. 66 (2016) 7–30.
[2] T. Conroy, F. Desseigne, M. Ychou, O. Bouche, R. Guimbaud, Y. Becouarn, A. Adenis, J.L. Raoul, S. Gourgou-Bourgade, C. de la Fouchardiere, J. Bennouna, J.B. Bachet, F. Khemissa-Akouz, D. Pere-Verge, C. Delbaldo, E. Assenat, B. Chauffert, P. Michel, C. Montoto-Grillot, M. Ducreux, U. Groupe Tumeurs Digestives of, P. Intergroup, FOLFIRINOX versus gemcitabine for metastatic pancreatic cancer, N. Engl. J. Med. 364 (2011) 1817–1825.
[3] D.D. Von Hoff, T. Ervin, F.P. Arena, E.G. Chiorean, J. Infante, M. Moore, T. Seay, S.A. Tjulandin, W.W. Ma, M.N. Saleh, M. Harris, M. Reni, S. Dowden, D. Laheru, N. Bahary, R.K. Ramanathan, J. Tabernero, M. Hidalgo, D. Goldstein, E. Van Cutsem, X. Wei, J. Iglesias, M.F. Renschler, Increased survival in pancreatic cancer with nab-paclitaxel plus gemcitabine, N. Engl. J. Med. 369 (2013) 1691–1703.
[4] D. Xie, K. Xie, Pancreatic cancer stromal biology and therapy, Genes Dis. 2 (2015) 133–143.
[5] M.H. Sherman, R.T. Yu, D.D. Engle, N. Ding, A.R. Atkins, H. Tiriac, E.A. Collisson, F. Connor, T. Van Dyke, S. Kozlov, P. Martin, T.W. Tseng, D.W. Dawson, T.R. Donahue, A. Masamune, T. Shimosegawa, M.V. Apte, J.S. Wilson, B. Ng, S.L. Lau, J.E. Gunton, G.M. Wahl, T. Hunter, J.A. Drebin, P.J. O'Dwyer, C. Liddle, D.A. Tuveson, M. Downes, R.M. Evans, Vitamin D receptor-mediated stromal reprogramming suppresses pancreatitis and enhances pancreatic cancer therapy, Cell 159 (2014) 80–93.
[6] P.P. Provenzano, C. Cuevas, A.E. Chang, V.K. Goel, D.D. Von Hoff, S.R. Hingorani, Enzymatic targeting of the stroma ablates physical barriers to treatment of pancreatic ductal adenocarcinoma, Canc. Cell 21 (2012) 418–429.
[7] B.C. Ozdemir, T. Pentcheva-Hoang, J.L. Carstens, X. Zheng, C.C. Wu, T.R. Simpson, H. Laklai, H. Sugimoto, C. Kahlert, S.V. Novitskiy, A. De Jesus-Acosta, P. Sharma, P. Heidari, U. Mahmood, L. Chin, H.L. Moses, V.M. Weaver, A. Maitra, J.P. Allison, V.S. LeBleu, R. Kalluri, Depletion of carcinoma-associated fibroblasts and fibrosis induces immunosuppression and accelerates pancreas cancer with reduced survival, Canc. Cell 25 (2014) 719–734.
[8] J. Prakash, Cancer-associated fibroblasts: perspectives in cancer therapy, Trends Canc. 2 (2016) 277–279.
[9] M.A. Shields, S. Dangi-Garimella, A.J. Redig, H.G. Munshi, Biochemical role of the collagen-rich tumour microenvironment in pancreatic cancer progression, Biochem. J. 441 (2012) 541–552.
[10] P.R. Kuninty, J. Schnittert, G. Storm, J. Prakash, MicroRNA targeting to modulate tumor microenvironment, Front Oncol 6 (2016) 3.
[11] H. Habisch, S. Zhou, M. Siech, M.G. Bachem, Interaction of stellate cells with pancreatic carcinoma cells, Cancers (Basel) 2 (2010) 1661–1682.
[12] M.V. Apte, J.S. Wilson, A. Lugea, S.J. Pandol, A starring role for stellate cells in the pancreatic cancer microenvironment, Gastroenterology 144 (2013) 1210–1219.
[13] K.M. Roach, C.A. Feghali-Bostwick, Y. Amrani, P. Bradding, Lipoxin A4 attenuates constitutive and TGF-beta1-dependent profibrotic activity in human lung myofibroblasts, J. Immunol. 195 (2015) 2852–2860.
[14] J.A. Chandrasekharan, N. Sharma-Walia, Lipoxins: nature's way to resolve inflammation, J. Inflamm. Res. 8 (2015) 181–192.
[15] C.N. Serhan, J. Savill, Resolution of inflammation: the beginning programs the end, Nat. Immunol. 6 (2005) 1191–1197.
[16] I.M. Fierro, C.N. Serhan, Mechanisms in anti-inflammation and resolution: the role of lipoxins and aspirin-triggered lipoxins, Braz. J. Med. Biol. Res. 34 (2001) 555–566.
[17] C.N. Serhan, M. Hamberg, B. Samuelsson, Lipoxins: novel series of biologically active compounds formed from arachidonic acid in human leukocytes, Proc. Natl. Acad. Sci. U. S. A. 81 (1984) 5335–5339.
[18] C.N. Serhan, K.A. Sheppard, Lipoxin formation during human neutrophil-platelet interactions. Evidence for the transformation of leukotriene A4 by platelet 12-lipoxygenase in vitro, J. Clin. Invest. 85 (1990) 772–780.
[19] J. Claria, C.N. Serhan, Aspirin triggers previously undescribed bioactive eicosanoids by human endothelial cell-leukocyte interactions, Proc. Natl. Acad. Sci. U. S. A. 92 (1995) 9475–9479.
[20] C.N. Serhan, N. Chiang, T.E. Van Dyke, Resolving inflammation: dual anti-inflammatory and pro-resolution lipid mediators, Nat. Rev. Immunol. 8 (2008) 349–361.
[21] C.N. Serhan, Pro-resolving lipid mediators are leads for resolution physiology, Nature 510 (2014) 92–101.
[22] K. Rodgers, B. McMahon, D. Mitchell, D. Sadlier, C. Godson, Lipoxin A4 modifies platelet-derived growth factor-induced pro-fibrotic gene expression in human renal mesangial cells, Am. J. Pathol. 167 (2005) 683–694.
[23] D. Mitchell, K. Rodgers, J. Hanly, B. McMahon, H.R. Brady, F. Martin, C. Godson, Lipoxins inhibit Akt/PKB activation and cell cycle progression in human mesangial cells, Am. J. Pathol. 164 (2004) 937–946.
[24] E. Borgeson, N.G. Docherty, M. Murphy, K. Rodgers, A. Ryan, T.P. O'Sullivan, P.J. Guiry, R. Goldschmeding, D.F. Higgins, C. Godson, Lipoxin A(4) and benzo-lipoxin A(4) attenuate experimental renal fibrosis, Faseb. J. 25 (2011) 2967–2979.
[25] S.H. Wu, Y.M. Zhang, H.X. Tao, L. Dong, Lipoxin A(4) inhibits transition of epithelial to mesenchymal cells in proximal tubules, Am. J. Nephrol. 32 (2010) 122–136.
[26] S.H. Wu, X.H. Wu, C. Lu, L. Dong, Z.Q. Chen, Lipoxin A4 inhibits proliferation of human lung fibroblasts induced by connective tissue growth factor, Am. J. Respir. Cell Mol. Biol. 34 (2006) 65–72.
[27] R. Bansal, E. Post, J.H. Proost, A. de Jager-Krikken, K. Poelstra, J. Prakash, PEGylation improves pharmacokinetic profile, liver uptake and efficacy of Interferon gamma in liver fibrosis, J. Contr. Release Offic. J. Contr. Release Soc. 154 (2011) 233–240.
[28] J. Schnittert, P.R. Kuninty, T.F. Bystry, R. Brock, G. Storm, J. Prakash, Anti-microRNA targeting using peptide-based nanocomplexes to inhibit differentiation of human pancreatic stellate cells, Nanomedicine 12 (12) (2017).
[29] P.R. Kuninty, L. Bojmar, V. Tjomsland, M. Larsson, G. Storm, A. Ostman, P. Sandstrom, J. Prakash, MicroRNA-199a and -214 as potential therapeutic targets in pancreatic stellate cells in pancreatic tumor, Oncotarget 7 (2016) 16396–16408.
[30] B. Costa-Silva, N.M. Aiello, A.J. Ocean, S. Singh, H. Zhang, B.K. Thakur, A. Becker, A. Hoshino, M.T. Mark, H. Molina, J. Xiang, T. Zhang, T.M. Theilen, G. Garcia-Santos, C. Williams, Y. Ararso, Y. Huang, G. Rodrigues, T.L. Shen, K.J. Labori, I.M. Lothe, E.H. Kure, J. Hernandez, A. Doussot, S.H. Ebbesen, P.M. Grandgenett, M.A. Hollingsworth, M. Jain, K. Mallya, S.K. Batra, W.R. Jarnagin, R.E. Schwartz, I. Matei, H. Peinado, B.Z. Stanger, J. Bromberg, D. Lyden, Pancreatic cancer exosomes initiate pre-metastatic niche formation in the liver, Nat. Cell Biol. 17 (2015) 816–826.
[31] M. Sarper, E. Cortes, T.J. Lieberthal, A. Del Rio Hernandez, ATRA modulates mechanical activation of TGF-beta by pancreatic stellate cells, Sci. Rep. 6 (2016) 27639.
[32] R. Kalluri, The biology and function of fibroblasts in cancer, Nat. Rev. Canc. 16 (2016) 582–598.
[33] A.I. Minchinton, I.F. Tannock, Drug penetration in solid tumours, Nat. Rev. Canc. 6 (2006) 583–592.
[34] P.A. Netti, D.A. Berk, M.A. Swartz, A.J. Grodzinsky, R.K. Jain, Role of extracellular matrix assembly in interstitial transport in solid tumors, Canc. Res. 60 (2000) 2497–2503.
[35] A. Neesse, K.K. Frese, T.E. Bapiro, T. Nakagawa, M.D. Sternlicht, T.W. Seeley, C. Pilarsky, D.I. Jodrell, S.M. Spong, D.A. Tuveson, CTGF antagonism with mAb FG-3019 enhances chemotherapy response without increasing drug delivery in murine ductal pancreas cancer, Proc. Natl. Acad. Sci. U.S.A. 110 (2013) 12325–12330.
[36] N. Ding, R.T. Yu, N. Subramaniam, M.H. Sherman, C. Wilson, R. Rao, M. Leblanc, S. Coulter, M. He, C. Scott, S.L. Lau, A.R. Atkins, G.D. Barish, J.E. Gunton, C. Liddle, M. Downes, R.M. Evans, A vitamin D receptor/SMAD genomic circuit gates hepatic fibrotic response, Cell 153 (2013) 601–613.
[37] C. Neuzillet, A. de Gramont, A. Tijeras-Raballand, L. de Mestier, J. Cros,

S. Faivre, E. Raymond, Perspectives of TGF-beta inhibition in pancreatic and hepatocellular carcinomas, Oncotarget 5 (2014) 78–94.
[38] E. Borgeson, N.G. Docherty, M. Murphy, K. Rodgers, A. Ryan, T.P. O'Sullivan, P.J. Guiry, R. Goldschmeding, D.F. Higgins, C. Godson, Lipoxin A(4) and benzo-lipoxin A(4) attenuate experimental renal fibrosis, Faseb. J. 25 (2011) 2967–2979.
[39] M.V. Apte, J.S. Wilson, A. Lugea, S.J. Pandol, A starring role for stellate cells in the pancreatic cancer microenvironment, Gastroenterology 144 (2013) 1210–1219.
[40] R.F. Hwang, T. Moore, T. Arumugam, V. Ramachandran, K.D. Amos, A. Rivera, B. Ji, D.B. Evans, C.D. Logsdon, Cancer-associated stromal fibroblasts promote pancreatic tumor progression, Canc. Res. 68 (2008) 918–926.
[41] M.A. Jacobetz, D.S. Chan, A. Neesse, T.E. Bapiro, N. Cook, K.K. Frese, C. Feig, T. Nakagawa, M.E. Caldwell, H.I. Zecchini, M.P. Lolkema, P. Jiang, A. Kultti, C.B. Thompson, D.C. Maneval, D.I. Jodrell, G.I. Frost, H.M. Shepard, J.N. Skepper, D.A. Tuveson, Hyaluronan impairs vascular function and drug delivery in a mouse model of pancreatic cancer, Gut 62 (2013) 112–120.